https://doi.org/10.5194/egusphere-2026-2322
Preprint. Discussion started: 20 May 2026
© Author(s) 2026. CC BY 4.0 License.

Calibration guidelines and a runoff-isotope module for lake proxy system modeling (PRYSM v2.0)

Rebecca G. Topness[1], Elizabeth K. Thomas[1], Michaela Fendrock[1,2], Gerard A. Otiniano[1]

[1]Department of Earth Sciences, University at Buffalo, Buffalo, NY, 14260, USA
[2]Alfred University, Alfred, NY, 14802, USA

Correspondence to: Rebecca G. Topness (rgtopnes@buffalo.edu)

Abstract. Lake sediments preserve information about past air temperature and precipitation, providing critical, real-world targets to validate climate models. However, these paleoclimate data encode information about multiple climate signals as well as lake dynamics, which makes comparison of paleoclimate data and model output challenging. Proxy system models (PSMs), or forward models that translate climate variables into proxy data, are tools for mechanistically interpreting paleoclimate data. PRYSM v2.0 is a PSM for paleoclimate data archived in lake sediments. Foundational to the accuracy of the PSM is a comprehensive understanding of the modern lake system supported by observations and meteorological forcing. However, two obstacles exist. First, lake water isotopes are the target of many proxies preserved in lake sediments, but the PSM does not have a built-in catchment model to aid simulation of lake water isotopes. Additionally, calibration of uncertain model parameters requires observations and expert knowledge about the lake, yet many sites are unmonitored. Here, we advance PSMs for lake sediment archives by integrating a simple runoff-isotope module that can be adapted to any lake and reproduce the seasonal timing and magnitude of two mid-latitude lakes with contrasting morphometry, hydrology, and mixing regimes. Using multi-year observational datasets from the lakes, we conduct model experiments that require the PSM to make water temperature and water δ^2H profile predictions when calibrated to a single observed profile, which mimics common observation collection challenges. For these lakes, we find that observations from the warm, ice-free season are most informative and constrain uncertain parameter values that best generalize to unseen data from other depths and years. Our framework for running and calibrating the PSM is available as open-source tools in Python, aiding the application of this PSM to the vast global database of lake sediment paleoclimate time series.

1 Introduction

Sediments accumulate over time in the bottom of lakes and preserve information about past air temperature and precipitation over thousands of years. These paleoclimate data can capture times in Earth's history when climate rapidly warmed, providing critical, real-world targets to validate climate models (Braconnot et al., 2012). In fact, time series generated from lake sediments currently comprise ~25% of paleoclimate databases (NOAA/World Data Service for Paleoclimatology & Neotoma, 2025). However, lake sediments preserve indirect observations of climate variables made from measurements of

https://doi.org/10.5194/egusphere-2026-2322
Preprint. Discussion started: 20 May 2026
© Author(s) 2026. CC BY 4.0 License.

physical, biological, and geochemical indicators. These paleoclimate "proxies" are often sensitive to multiple climate variables and additionally to lake dynamics (Castañeda and Schouten, 2011). Therefore, interpreting variables useful for climate model validation (i.e. rainfall amount, air temperature) from lake sediments can be challenging.

The development of PRYSM v2.0, a proxy system model (PSM) for lake sediment archives, allows for mechanistic interpretation of paleoclimate data and facilitates comparisons with climate model output (Dee et al., 2018). PSMs are process-based forward models that convert climate variables (i.e. rainfall amount, air temperature) into lake and/or paleoclimate data units (Evans et al., 2013). PSMs are now commonly used tools in paleoclimatology, with PSMs available for a variety of proxy systems (e.g. ice cores, tree rings, cave deposits, corals). Unlike transfer functions, which hinge on certain assumptions regarding how proxies respond to climate forcing (e.g. Zhao et al., 2021), PSMs simulate each step in the encoding of climate variables within a proxy, allowing for non-linear responses and uncertainty quantification (Dee et al., 2018).

PSMs have been used to interpret paleoclimate data from lake sediments in several ways, from simple climate sensitivity experiments to the translation of climate model outputs and more complex Bayesian inference frameworks. Testing a lake's sensitivity to climate forcing can elucidate possible mechanisms for observed variability in a paleoclimate proxy time series. After calibration of the PSM to the modern lake system, individual changes in climate forcing (e.g. increase precipitation amount, decrease air temperature, or decrease shortwave radiation) are prescribed and the lake response quantified (Acharya et al., 2025; Cluett et al., 2023; Corcoran et al., 2021; Holtzman et al., 2025; Hostetler and Benson, 1990; Hostetler, 1991; Morrill et al., 2001). Similarly, PSMs are powerful tools for translating climate model outputs into lake and/or climate variables, which can then be directly compared to proxy time series in identical units and model-data discrepancies identified. This involves forcing a PSM of the modern lake system with paleoclimate model simulations and comparing relevant PSM outputs with proxy reconstructions (Dee et al., 2021a; Jones and Dee, 2018; Longo et al., 2020; Marshall et al., 2025; Morrill et al., 2019). Another application of PSMs is within Bayesian inference frameworks, in which a calibrated PSM converts a wide range of climate scenarios into simulated proxy data (Guiot et al., 2009; Parnell et al., 2015). Climate forcings are perturbed until simulated and observed proxy data agree, resulting in a proxy time series that is translated into climate variables, including uncertainty. This Bayesian approach to obtain quantitative paleoclimate information has been applied to pollen records from lake sediment archives, as terrestrial plants respond to atmospheric variables (e.g. Guiot et al., 2000; Haslett et al., 2006; Parnell et al., 2016). Yet, application to other lake sediment paleoclimate proxies (such as aquatic plant leaf waxes and branched dialkyl glycerol tetraethers) that grow within the water column may require simulation of the lake system's response to climate (Casteñeda and Schouten, 2011). Foundational to any of these applications is a comprehensive understanding of the lake system based on modern observations and meteorological forcing.

However, two obstacles hinder the broad use of PSMs to interpret lake sediment archives:

https://doi.org/10.5194/egusphere-2026-2322
Preprint. Discussion started: 20 May 2026
© Author(s) 2026. CC BY 4.0 License.

(1) Lake water isotopes (stable isotopes of oxygen and hydrogen, $\delta^{18}O$ and $\delta^{2}H$) are the target of many proxy observations from lake sediments, such as aquatic plant leaf waxes and carbonates (Dee et al., 2023). However, long-term, continuous observations of precipitation and runoff isotope values needed to force the PSM to simulate lake water isotope values are rare (IAEA/WMO, 2015; Birkel et al., 2025). Furthermore, the PSM does not have a built-in catchment model that would aid in the simulation of both runoff and runoff isotope values (Dee et al., 2018).

(2) The PSM requires calibration of several lake-specific parameters and substantial user set-up. Previous studies rely on published limnological, and often meteorological, observational datasets to meet this goal (Dee et al., 2021b; Hostetler, 1991; Hostetler and Benson, 1994; Longo et al., 2020; Marshall et al., 2025; Morrill et al., 2019; Sae-Lim et al., 2025). This can be difficult if time and resource limitations, or remote study sites, preclude collection of continuous observations. For example, when paleoclimatologists collect a lake sediment core in the field, the time spent at each site may only be a few days, limiting observations to that window (e.g. Corcoran et al., 2021). Sometimes temperature and lake level sensors may be deployed and retrieved at a later date, but this is not always possible at remote sites (e.g. Acharya et al., 2025; Cluett et al., 2023), nor at sites where lake sediments have already been collected and paleoclimate proxy time series generated. No widely deployable sensor currently exists to continuously monitor lake water isotope values, so observations are limited to when water samples can be manually collected (e.g. Holtzman et al., 2025).

We address these challenges of applying PSMs to lake sediment archives by developing tools and guidelines to streamline set-up and calibration of PRYSM v2.0. Our objectives are to (1) build and test a simple, flexible runoff module to aid simulation of lake water isotopes and (2) identify the most informative sampling periods and abundance of observations necessary to achieve reliable and robust model calibration. To do this, we use the PSM to simulate two mid-latitude lakes, Red Pond and Bear Lake, with contrasting morphometry, hydrology, and mixing regimes. We focus on lake water temperature and $\delta^{2}H$ values, which are two variables encoded within proxies in lake sediments. Tools in Python for running and calibrating the PSM are organized in a GitHub repository (https://github.com/rgtopness/lake-psm-calibration/), with a snapshot of this repository stored on Zenodo (Topness et al., 2025a).

2 Model descriptions

The PRYSM v2.0 proxy system modeling framework is made up of four distinct submodels. Each submodel describes a set of processes that transform the climate signal before it is encoded into a proxy within lake sediments. For example, the "environment" submodel simulates a lake's response to climate and the "sensor" submodel represents how a proxy responds to the change in its environment, i.e., the lake (see Dee et al., 2018 for more details on the four submodels). Here we focus only on the environment submodel because output from this submodel drives the other submodels, and the environment

https://doi.org/10.5194/egusphere-2026-2322
Preprint. Discussion started: 20 May 2026
© Author(s) 2026. CC BY 4.0 License.

submodel requires the most lake-specific set-up and calibration. In the following section, we also describe the runoff module, which generates variables that force the environment submodel.

2.1 PRYSM v2.0 environment submodel

The environment submodel is a one-dimensional lake energy, water, and isotopic balance model from Hostetler and Bartlein (1990) with modifications by Morrill et al. (2019) and further updates described here. The model calculates lake energy and isotopic balance using physically based equations. The vertical transfer of heat happens through convective mixing when density inversions exist and eddy diffusion from mixing by wind. Isotopic fractionation occurs during evaporation and is determined by wind speed, lake water temperature and isotope value, and the relative humidity and water vapor isotope value of the atmospheric boundary layer (Hostetler and Benson, 1994). The model allows for fractional lake ice coverage. In our version of the model, we update treatment of lake water stable isotopes when ice is present, ensuring ice cover stops isotopic exchange between the water and the atmosphere. In this model, runoff is routed into the mixed layer and does not change lake water temperature (Hostetler and Benson, 1994).

The environment submodel requires seven meteorological input variables: air temperature, humidity, wind speed, shortwave radiation, longwave radiation, surface pressure, and precipitation amount. Simulation of lake water isotope values and water balance necessitates five additional meteorological variables: precipitation δ^2H and $\delta^{18}O$ values, runoff amount, and runoff δ^2H and $\delta^{18}O$ values. Precipitation isotope values can be derived from observations or from modeled values, such as the Online Isotopes in Precipitation Calculator (Bowen et al., 2005; Bowen et al., 2017; Welker et al., 2000). The input frequency of meteorological variables is flexible to any time step. In this study, we ran the environment submodel on a daily time step, but hourly, 6-hourly, monthly, etc. is also possible. The environment submodel interpolates inputs, if needed, to the model time step of 30 minutes. Outputs are saved on a daily time step regardless of meteorological input frequency.

In addition to catchment area, lake area for each depth slice, and maximum depth, ten lake-specific parameters must be prescribed in the model (Table 1). Because values for several of these parameters are difficult to measure in the field, calibration is necessary.

https://doi.org/10.5194/egusphere-2026-2322
Preprint. Discussion started: 20 May 2026
© Author(s) 2026. CC BY 4.0 License.

Table 1: Description of lake-specific and runoff parameters with ranges used for Latin Hypercube sampling to generate an ensemble of 1000 simulations. Ranges of sensitive parameters (calibrated range is significantly different from the range of 1000 simulations) in the runoff module calibration were narrowed prior to simulating lake water temperature and δ^2H profiles. Sensitive parameters across calibration to all observational datasets are shown in bold text. Parameters are unitless unless otherwise noted.

Parameter name	Parameter description	Units	Range for 1000 runoff simulations	Range for 1000 runoff + lake simulations	Source
Environment submodel					
cdrn	Neutral drag coefficient			**$1x10^{-3}$ to $2.5x10^{-3}$**	Morrill et al. (2019)
eta	Shortwave extinction coefficient	m^{-1}		**0.3 to 4**	Secchi disk depth observations, Bigham Stephens et al. (2015)
alb_snow	Albedo of non-melting snow			**0.7 to 0.9**	Morrill et al. (2019)
alb_slush	Albedo of melting snow			0.4 to 0.7	Morrill et al. (2019)
d18Oa	$\delta^{18}O$ value of atmospheric boundary layer water vapor advected from adjacent land	‰ VSMOW		**-27.55 to -11.03**	Santos et al. (2012)
d2Ha	δ^2H value of atmospheric boundary layer water vapor advected from adjacent land	‰ VSMOW		**-210.4 to -78.24**	Santos et al. (2012)
f	Fraction advected air from adjacent land above lake			**0 to 1**	Morrill et al. (2019)
alb_sed	Albedo of lake sediment			not simulated	
csed	Specific heat of sediment	$Jm^{-3}K^{-1}$		not simulated	
condsed	Thermal conductivity of sediment	$Js^{-1}m^{-1}K^{-1}$		not simulated	
Runoff module					
melt_ratio	Fraction accumulated precipitation converted to runoff		0.05 to 1	0.05 to 1	
rsm_ratio	Fraction of snowmelt converted to runoff		0.05 to 1	0.05 to 1	
glacier_flux	Runoff amount per hectare basin area; set to 0 if no glacier in catchment	mm	0	0	
p	Period for Gaussian weighted moving average calculation		0 to 100	0 to 100	
s	Sigma for Gaussian weighted moving average		**0 to 10**	0.87 to 1	
thaw_threshold	Number of days above freezing required to start runoff	days	**0 to 7**	0 to 2	
freeze_threshold	Number of days below freezing required to stop runoff	days	0 to 7	0 to 7	
rp_ratio_freeze	Runoff to precipitation ratio for when air temperature is at or below freezing ($T \leq 0°C$)		**0 to 1**	0.15 to 0.90	
rp_ratio_cold	Runoff to precipitation ratio for cold air temperatures but above freezing ($0°C < T \leq 10°C$)		**0 to 1**	**0.27 to 1**	
rp_ratio_mild	Runoff to precipitation ratio for mild air temperatures ($10°C < T \leq 20°C$)		**0 to 1**	**0.16 to 0.69**	
rp_ratio_warm	Runoff to precipitation ratio for warm air temperatures ($20°C < T$)		**0 to 1**	0.02 to 0.32	

https://doi.org/10.5194/egusphere-2026-2322
Preprint. Discussion started: 20 May 2026
© Author(s) 2026. CC BY 4.0 License.

135

2.2 Runoff module

We adapt a simple runoff module from Cluett (2021) to be flexible to any catchment. The module calculates runoff amount and runoff δ^2H and $\delta^{18}O$ values based on daily air temperature, precipitation amount, and precipitation δ^2H and $\delta^{18}O$ values. The module also estimates the amount of snow accumulated in the catchment and its δ^2H and $\delta^{18}O$ values, which are not
140 required to force the environment submodel but could be useful to compare with observations, if available.

The runoff module has 11 tunable parameters that control the runoff amount and isotope value at any given time step (Table 1). Runoff-to-precipitation ratios describe the proportion of precipitation that becomes runoff rather than evaporating or being stored in soils. The model uses four distinct runoff-to-precipitation ratio parameters, each triggered by a specific air
145 temperature range (which can be tailored to the site by the user) to represent different hydrological regimes. To simulate gradual freeze-up in the fall and thaw in the spring, the "thaw_threshold" and "freeze_threshold" parameters dictate the number of days needed to start or stop runoff, respectively. If snow has accumulated in the catchment, the "melt_ratio" controls the fraction of accumulated snow that is converted to meltwater each time step. The "rsm_ratio" partitions the meltwater between immediately contributing to runoff and short-term storage in snowpack. A fraction of meltwater from the
150 previous accumulation contributes to runoff in the current time step, while the remaining fraction (1 - "rsm_ratio") is trapped and released with a one-time step delay. If a glacier is present in the catchment, the "glacier_flux" parameter can be set, which supplies an amount of meltwater in mm from that source relative to the catchment area. Runoff δ^2H and $\delta^{18}O$ values from glacial meltwater default to the minimum precipitation isotope value supplied in the meteorological input file, or can be specified by the user.

155

Runoff amount in mm at each time step is calculated from the contributing water sources (current precipitation amount that becomes runoff, meltwater from recent accumulation, the prescribed glacier flux, and meltwater from older stored accumulation in the catchment) as follows, where *i* is the *i*th time step.

(1) $$Runoff_i = (Precip_i * rp_{ratio}) + (Acc_{i-1} * melt_{ratio} * rsm_{ratio}) + (Acc_{i-2} * melt_{ratio} * (1 - rsm\_ratio)) +$$
160 $$glacier\_flux$$

At each time step where air temperature and precipitation amount result in runoff into the lake, runoff δ^2H and $\delta^{18}O$ values are calculated as a mixture of each of the contributing water sources described above, where each source's δ^2H and $\delta^{18}O$ values are weighted by its contribution to total runoff amount at that time step.

(2) $$\delta^2 HRunoff_i = \left(\frac{Precip_i * rp\_ratio * \delta^2 HPrecip_i}{Runoff_i}\right) + \left(\frac{Acc_{i-1} * melt\_ratio * rsm\_ratio * \delta^2 HAcc_i}{Runoff_i}\right) +$$
165 $$\left(\frac{Acc_{i-2} * melt\_ratio * (1-rsm\_ratio) * \delta^2 HAcc_{i-2}}{Runoff_i}\right) + \left(\frac{glacier\_flux * \delta^2 HGlacier_i}{Runoff_i}\right)$$

https://doi.org/10.5194/egusphere-2026-2322
Preprint. Discussion started: 20 May 2026
© Author(s) 2026. CC BY 4.0 License.

(3) $$\delta^{18}ORunoff_i = \left(\frac{Precip_i * rp\_ratio * \delta^{18}OPrecip_i}{Runoff_i}\right) + \left(\frac{Acc_{i-1} * melt\_ratio * rsm\_ratio * \delta^{18}OAcc_i}{Runoff_i}\right) + \left(\frac{Acc_{i-2} * melt\_ratio * (1-rsm\_ratio) * \delta^{18}OAcc_{i-2}}{Runoff_i}\right) + \left(\frac{glacier\_flux * \delta^{18}OGlacier_i}{Runoff_i}\right)$$

These runoff module outputs force the environment submodel, which converts and transforms input runoff amounts into volume in m^3 by multiplying amounts by the prescribed catchment area.

3 Methods

3.1 Study sites

We simulate two lakes located in western New York State with contrasting morphometry, hydrology, and mixing regimes (Fig. 1). Red Pond (42.1333°N, -78.9128°W) is a small meromictic kettle pond with no channelized inflow or outflow, and a maximum depth of 18 meters. The lake surface area is approximately 1 hectare, and the 10-hectare catchment is forested and steeply sloping. Bear Lake (42.3470°N, -79.3840°W) is a large, dimictic lake with two inflows and one outflow that are channelized and constantly flowing. The maximum depth of 8 meters is shallow compared to Red Pond. Bear Lake's surface area is 49 hectares with a 2600-hectare catchment. Both lakes experience ice cover during winter, with ice-off occurring late March to early April and ice-on mid-December to mid-January. Because the lakes are within two hours by car from the University at Buffalo's campus, frequent monitoring was possible.

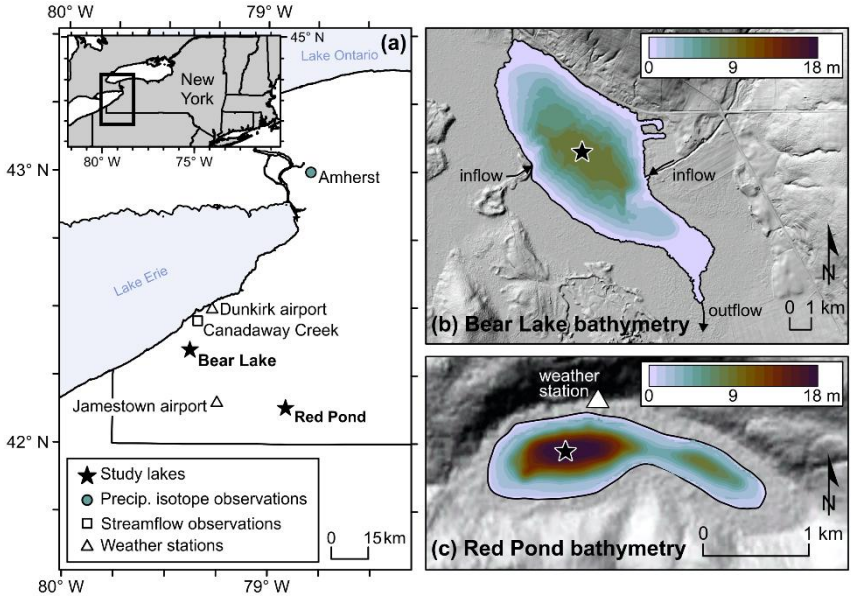

Figure 1: Maps of study area. (a) Map of western New York State showing locations of study lakes, as well as sites of precipitation isotope observations, streamflow observations, and weather stations relevant to model inputs. Inset map shows location in eastern North America. Bathymetric maps of (b) Bear Lake and (c) Red Pond showing location of monitoring and moorings (stars). 2 m LiDAR from https://data.gis.ny.gov/. Colormap from Crameri et al. (2020).

https://doi.org/10.5194/egusphere-2026-2322
Preprint. Discussion started: 20 May 2026
© Author(s) 2026. CC BY 4.0 License.

3.2 Observational datasets

We collected multi-year lake water δ^2H and temperature observations to calibrate the environment submodel for Red Pond and Bear Lake (Table 2; Topness et al. 2026b, c).

Most lake water temperature observations were measured continuously by thermistor strings. We deployed HOBO UTBI-001 temperature loggers (Red Pond: approximately 1, 2, 8, and 18 m; Bear Lake: approximately 1 and 7m; temperature accuracy: ±0.21 °C) and a HOBO U20L-01 temperature and water level logger (Red Pond: 4.6 m; Bear Lake: 4 m; temperature accuracy: ±0.44 °C) to monitor at 30-minute intervals. To correct for slight changes in logger depths between deployment periods, we calculated water pressure from the water level logger and estimated the distance of each instrument (which is fixed) relative to the location of the water level logger on the string. We computed daily average temperatures only for days where there are observations over the full day (i.e. no half-days) at each depth, which best matches environment submodel output (daily average of each 1-meter depth layer). We also collected temperature profiles with measurements at every meter from surface to bottom using a Yellow Spring Instruments EXO3 multiparameter water quality sonde (temperature accuracy: ±0.01 °C; Fig. S1). For Bear Lake, we supplemented our observations with temperature profiles from the New York State Department of Environmental Conservation's Division of Water Monitoring Data Portal (NYSDEC, 2025).

To monitor lake water δ^2H and $\delta^{18}O$ values, we collected lake water samples at depths of 1, 4, 7, 16, and 18 m at Red Pond, due to its depth and stability, and every meter at Bear Lake using a Nansen bottle (Aquatic Research Instruments; Fig. S1). We stored samples at 4 °C in capped and Parafilm-sealed 4 mL glass vials with no head space. We filtered water samples using 0.2 µm hydrophilic Teflon filters into 2 mL glass vials before analysis. We measured δ^2H and $\delta^{18}O$ using a Picarro L2130-i Wavelength-Scanned Cavity-Ring Down Spectrometer with a V1102-i vaporization module and CTC Analytics Prep and Load autosampler at the University at Buffalo Organic and Stable Isotope Biogeochemistry Laboratory (UB OSIBL). We measured each sample four times, discarding the first injection, and reported the average value of the last three injections. We calibrated measured values using UB OSIBL standards that span a range of -265.9 to +21.4 ‰ for δ^2H and -33.61 to +12.41 for $\delta^{18}O$. The UB OSIBL standards were calibrated using primary standards (GISP, VSMOW2, SLAP2) from the International Atomic Energy Agency (IAEA). We corrected for memory and drift following Van Geldern and Barth (2012). Average standard deviations of replicate measurements were 0.47 ‰ for δ^2H and 0.09 ‰ for $\delta^{18}O$. We reported results using delta notation in per mille (‰) relative to Vienna Standard Mean Ocean Water (VSMOW).

We assess the runoff module's performance using daily average streamflow observations from Canadaway Creek (42.4506 N, -79.3504 W; USGS, 2025). We use these observations for runoff module calibration because Canadaway Creek is the closest monitored stream to our study sites that is not dammed (Fig. 1a). To compare with simulated runoff amounts, we

https://doi.org/10.5194/egusphere-2026-2322
Preprint. Discussion started: 20 May 2026
© Author(s) 2026. CC BY 4.0 License.

divided the daily average streamflow observations by the drainage area that sources the stream's monitoring gauge (Table 2). We only included observations that have been accepted for publication by USGS.

Table 2: Observational data used for bias correction, forcing, calibration, and validation.

Site name	Location (latitude, longitude, elevation or area)	Period analyzed	Variables used	Source
Bias correction				
Red Pond weather station	42.1336 N, -78.9126 W 430 m	10 Jun 2022–14 Nov 2025	Air temperature Dewpoint temperature	This study
Jamestown airport (NCEI 72523504720)	42.15 N, -79.25 W 520 m	1 Jan 2006–25 Aug 2025	Air temperature Dewpoint temperature Wind speed Precipitation amount Surface pressure	NOAA NCEI (1999)
Dunkirk airport (NCEI 74498999999 and NCEI 74498914747)	42.4932 N, -79.27623 W 200 m	3 Jan 2005–27 Aug 2025	Air temperature Dewpoint temperature Wind speed Precipitation amount Surface pressure	NOAA NCEI (1999)
Precipitation δ^2H and $\delta^{18}O$ forcing				
Amherst precipitation gauge	43.0000 N, -78.7915 W 222 m	12 Aug 2014–12 Dec 2025	Event-based precipitation δ^2H and $\delta^{18}O$ values	Corcoran et al. (2019)
Borden, Ontario, Canada flux tower	44.3167 N, -79.9333 W 250 m	1 May 2009–30 Aug 2009	Atmospheric water vapor δ^2H and $\delta^{18}O$ values	Santos et al. (2012); Wei et al. (2019)
Calibration and validation				
Canadaway Creek (USGS 4213376)	42.4506 N, -79.3504 W 85.21061 km^2 area	10 Aug 2017–31 Dec 2025	Streamflow	USGS (2025)
Red Pond	42.1333 N, -78.9128 W 430 m	6 Nov 2021–15 Nov 2025	Water temperature profiles (n = 1256)	This study
		11 Sept 2021–15 Nov 2025	Water δ^2H and $\delta^{18}O$ profiles (n = 16)	
Bear Lake	42.3470 N, -79.3840 W 400 m	25 Jun 2012–28 Feb 2025	Water temperature profiles (n = 120)	This study; NYS DEC (2025)
		22 Apr 2024–17 Nov 2024	Water δ^2H and $\delta^{18}O$ profiles (n = 7)	

3.3 Model inputs

We force the environment model with daily ERA5 Global Reanalysis Data from 1994 to 2025 (Hersbach et al., 2020; Hersbach et al., 2023). We extract and average data from the four grid cells that intersect the lake and catchment area (Red Pond: (42°N, -79°W), (42°N, -78.75°W), (42.25°N, -79°W), (42.25°N, -78.75°W) and Bear Lake: (42.25°N, -79.50°W), (42.25°N, -79.25°W), (42.50°N, -79.50°W), (42.50°N, -79.25°W). We use 6-hourly resolution for all variables except for

https://doi.org/10.5194/egusphere-2026-2322
Preprint. Discussion started: 20 May 2026
© Author(s) 2026. CC BY 4.0 License.

accumulated variables (precipitation amount, longwave radiation, shortwave radiation), which we download at hourly resolution and then sum to accurately represent daily totals (Fig. S2).

Quantile-mapping is often used to remove bias from reanalysis data (e.g. Morrill et al., 2019), but we do not correct model inputs due to minimal differences with catchment and nearby meteorological observations (Table 2). At Red Pond, we monitored daily air temperature and relative humidity using a HOBO U23-001A Pro v2 weather station (temperature accuracy: ±0.2 °C; relative humidity accuracy: ±2.5 %; Topness et al., 2026b). Comparison of Red Pond ERA5 air temperature and relative humidity to our weather station observations from June 2022 to November 2025 reveal the differences were insignificant (Figs. S3 and S4). While wind speed observations from Jamestown, New York (NOAA NCEI, 1999) are significantly higher than ERA5 ($KS = 0.141$, $p < 0.001$), we do not correct this variable because Red Pond's location in a kettle hole surrounded by a forested catchment creates low wind speeds at the lake. Observations from Dunkirk, New York and ERA5 variables for Bear Lake show some significant differences (NOAA NCEI, 1999; Figs. S5 and S6). Air temperature and wind speed ($KS = 0.068$, $p < 0.001$ and $KS = 0.152$, $p < 0.001$, respectively) are higher than ERA5 in the 90th percentiles. However, we do not quantile-map due to large (~200 meters) elevation differences between Dunkirk and Bear Lake.

Because precipitation isotope values are not variables available in this reanalysis dataset, we followed previous studies (Corcoran et al., 2021; Holtzman et al., 2025; Jones and Dee, 2018) and use an amount-weighted monthly average climatology to force the environment model for water isotope balance. We use event-based observations from Amherst, New York spanning August 2014-December 2025 (Corcoran et al., 2019) to build our monthly climatology. While this simplifies the system (i.e. no variability among years), it is necessary because decades-long, continuous precipitation isotope observations are rare (IAEA/WMO, 2015).

We estimate the lake surface and catchment area for both lakes using Google Earth. We surveyed bathymetry using a Humminbird Fishfinder device and plotted results using Autochart software (https://humminbird.johnsonoutdoors.com/us/learn/mapping/autochart). Because Red Pond has two basins separated by a sill that is shallower than the maximum summer mixolimnion (4 m depth), we only simulate the larger, western basin from which we collected observations (Fig. 1c). We set the vertical layer thickness parameter to 1 meter ($dz = 1.0$), following applications of this model to lakes with similar depths (Martynov et al., 2010; Morrill et al., 2019). For both lakes, we prescribe initial conditions for lake water temperature, salinity, and δ^2H and $\delta^{18}O$ values as observed profile averages. We perform a model spin-up by simulating ten years of 1994 conditions, then save outputs from 1995 to 2025.

https://doi.org/10.5194/egusphere-2026-2322
Preprint. Discussion started: 20 May 2026
© Author(s) 2026. CC BY 4.0 License.

3.4 Establishing parameter ranges

An important step for calibration of model parameters is defining the sampling space (Mai, 2023). We sample from a wide range while ensuring possible values are physically possible for the study lakes (Table 1). We use suggested ranges from Dee et al. (2018) for all lake-specific parameters, excluding the shortwave extinction coefficient, which is a critical parameter for accurately simulating water temperature (Dee et al., 2018; Morrill et al., 2019). Secchi disk depth observations from Red Pond and Bear Lake, and for 388 lakes in New York State (which we convert using $1.57/Z_{SD} = \eta$; Dee et al., 2018) support higher values for the shortwave extinction coefficient (Bigham Stephens et al., 2015) (Fig. S7). Therefore, we update the recommended range from 0.1-1.0 to 0.3-4.0 m^{-1}. We do not simulate thermal impacts from bottom sediments, so do not include the albedo, specific heat, and thermal conductivity of sediment parameters. See Morrill et al. (2019) and https://github.com/carriemorrill/lake-model/ for more details on sediment heat parameters.

We establish parameter ranges for $\delta^{18}O$ values of atmospheric water vapor above the lake using minimum and maximum summer (June-August) observations from Borden, Ontario, Canada (44.3167 N, -79.9333 W; Santos et al., 2012) available through the Stable Water Vapor Isotopes Database (Wei et al., 2019). We use this site because of its proximity to our study lakes and similar geographic position downwind from a Laurentian Great Lake (Lake Huron). We calculate δ^2H values of atmospheric water vapor above the lake based on the Global Meteoric Water Line relationship ($\delta^2H = 8*\delta^{18}O + 10$). This step removes the need to provide ranges for both δ^2H and $\delta^{18}O$ values and ensures these parameters are physically linked. We start with the full range of runoff parameter values as defined by Cluett (2021), and set all runoff-to-precipitation ratios from 0 to 1 (Table 1). We do not use glacier parameters for these simulations because no glaciers exist in the modern lake catchments.

3.5 Runoff module calibration

Given our goal to accurately simulate lake water isotope values, we aim to reproduce the seasonal distribution of runoff amount for our study sites. Therefore, we calibrate and validate the runoff module using monthly summed runoff amounts estimated using Canadaway Creek streamflow observations (USGS, 2025). Following Morrill et al. (2019), we used even years for calibration and odd years for validation, after confirming the distribution of values in each period are comparable with a Kolmogorov-Smirnov test. We generate 1000 runoff module simulations with parameter sets selected using Latin Hypercube sampling across the full range of runoff parameter values (Table 2). We evaluate calibration and validation periods using criteria suggested by Moriasi et al. (2007) for monthly streamflow: Nash-Sutcliffe Efficiency (NSE) > 0.50, percent bias < 25%, and ratio of the root-mean-square error to the standard deviation of measured data (RSR) <= 0.7. We narrow ranges of sensitive runoff parameters for further use in lake model simulations to ensure water isotope values are supported by realistic runoff amounts for the region.

https://doi.org/10.5194/egusphere-2026-2322
Preprint. Discussion started: 20 May 2026
© Author(s) 2026. CC BY 4.0 License.

3.6 Environment submodel calibration

Calibration of the environment submodel can require hundreds or thousands of iterations to test possible values of unknown parameters, which are somewhat computationally costly. We establish a parallel processing framework that can be run on a laptop to streamline calibration of lake-specific and runoff parameters. As a general overview of the workflow, the user supplies a comma-separated values (CSV) file with parameter ranges, from which the user can generate the desired number of parameter sets (i.e. 1000) with values selected using Latin Hypercube Sampling (Virtanen et al., 2020). The runoff module automatically runs, using parameter sets to calculate runoff variables and append them to meteorological input files. Completed meteorological input files and compiled lake models are placed in separate folders with unique labels. Next, compiled models are run and output files saved (as netCDFs or text files) for further analysis. Models run in parallel to speed up run times (default is five models run simultaneously). For example, parallelization allows 1000 models each simulating 30 years on a daily time step to complete in less than one hour on a laptop, compared to approximately seven hours when run sequentially.

We use this framework to generate a 1000-member ensemble of daily water-temperature and water-isotope profile simulations with parameter sets sampled across the full range of lake model parameters and the narrowed range for runoff parameters (Table 1). We evaluate each simulation's performance by calculating root-mean-square error (RMSE) between observed and modeled values across all dates and depths, where *n* is the total number of observations.

$$RMSE = \sqrt{\frac{1}{n}\sum_{i=1}^{n}(Modeled_i - Observed_i)^2} \quad (4)$$

We also calculate bias to investigate the direction of error, where *n* is the total number of observations. We do not use bias as a metric for calibration.

$$Bias = \frac{1}{n}\sum_{i=1}^{n}(Modeled_i - Observed_i) \quad (5)$$

Modeled values are output as averages of each 1-meter depth, so we treat modeled values as layer midpoints and linearly interpolate modeled values to observation depths prior to calculating RMSE. We also check that the approximate timing of ice-off is realistic for the lakes based on local ice cover observations. We select the 30 simulations with the lowest RMSE as our calibrated ensemble.

3.7 Model experiments

We conduct experiments to assess the performance of the PRYSM v2.0 environment submodel using calibration datasets that mimic common observation collection challenges. The experiments require the lake model to make water temperature or water δ^2H value predictions for the lakes when calibrated using a single observed profile. This is a realistic scenario reflective of short field seasons (e.g. a few days) at remote study sites. We aim to identify which season's observations are most informative and if the minimum number of observations (one profile) is enough to set-up the model so it accurately

https://doi.org/10.5194/egusphere-2026-2322
Preprint. Discussion started: 20 May 2026
© Author(s) 2026. CC BY 4.0 License.

predicts unseen data. To meet that end, we evaluate the success of each calibration through validation against all other observational profiles available for that lake. By testing two lakes with contrasting morphometries and mixing regimes, we can investigate if those lake characteristics have any control over the optimal sampling window.

Our experiments use profile observations from Bear Lake and Red Pond and divide the datasets into one calibration profile for each date. Because some dates have a profile made up of observations from every meter, while others only include 3-4 observations between the lake surface and the bottom, we subset the observational datasets so each profile on each date includes the same number of observations spaced approximately evenly from lake surface to bottom. For Bear Lake, each date includes observations at three depths between 0 m and 8 m; for Red Pond, each date includes observations at four depths between 0 m and 18 m. For Red Pond we target 1.5m, 4m, 8m, and 17m and for Bear Lake we target 1m, 4m, and 7m. Dates are included if observations exist on that date that are equal or less than 1 m away from the target depths. This means that each date has a profile that captures key physics (near-surface, thermocline, bottom) and equalizes the number of points in the calibration on each date so model performance can be compared (Figs. S8 and S9). For Red Pond, this results in 1254 water temperature profiles and 15 water δ^2H profiles for the experiments. For Bear Lake, this results in 79 water temperature profiles and 6 water δ^2H profiles for the experiments.

We use the 1000 daily lake water temperature and δ^2H profile simulations previously generated and described as a reasonable estimation of parameter uncertainty at a sparsely monitored lake. We calibrate each date by choosing the 30 best-performing (lowest RMSE) simulations from the 1000 total simulations. We evaluate the informativeness of each date's calibration by using observations from all remaining dates and depths as validation. As before, we calculate RMSE as a measure of model performance and to craft guidelines for the most informative sampling season.

4 Results

4.1 Runoff module performance

The PSM does not have a built-in catchment model that would aid in the simulation of both runoff and runoff isotope values (Dee et al., 2018). To address this, we integrate and test a runoff-isotope module with the goal to create plausible runoff amounts and runoff isotope values to force the environment submodel. The calibration period statistics for 21 simulations met the criteria described above for monthly streamflow. Module performance for these simulations remained within the criteria for the validation period. These simulations capture the seasonal timing and amount of runoff for our study sites (Fig. 2), with low runoff in summer months and rain and snowmelt increasing runoff amount in the winter and spring (Hrycik et al., 2024). We identify parameters as sensitive if their calibrated range was significantly ($p < 0.05$) different from the uniform, original parameter range via Kolmogorov-Smirnov test. Sensitive runoff parameters were the "thaw_threshold", "s"

https://doi.org/10.5194/egusphere-2026-2322
Preprint. Discussion started: 20 May 2026
© Author(s) 2026. CC BY 4.0 License.

(sigma for the Gaussian weighted moving average), and "rp_ratio_freeze", "rp_ratio_cold", "rp_ratio_mild", and "rp_ratio_warm" (Table 1).

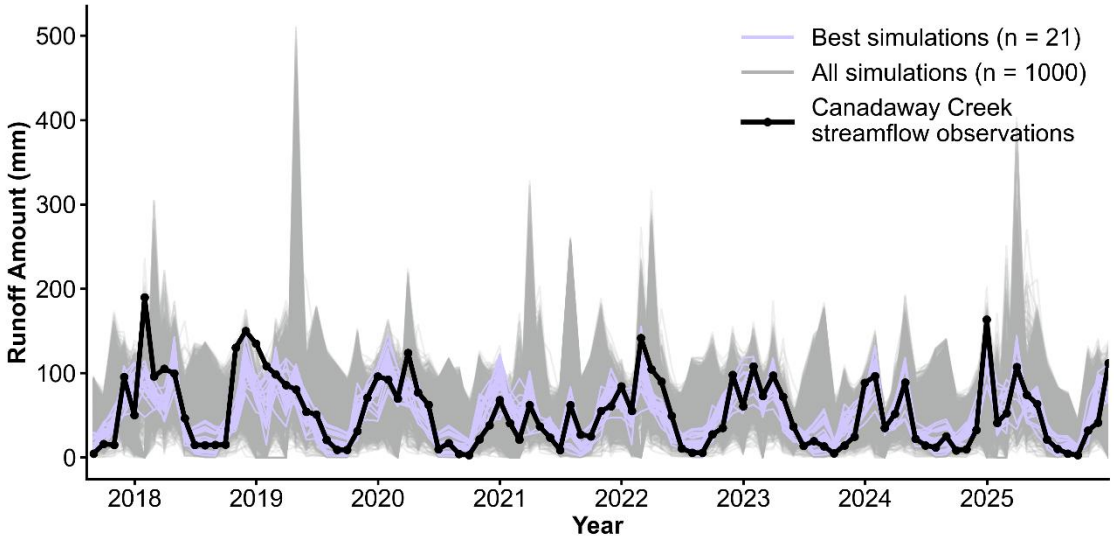

Figure 2: Results of runoff module calibration to drainage area-normalized monthly streamflow from Canadaway Creek (USGS, 2025). We identified the 21 best simulations using criteria from Moriasi et al. (2007).

4.2 Environment submodel performance

The environment submodel accurately reproduces our observed water temperature profiles from Bear Lake and Red Pond, two lakes with contrasting mixing regimes. Model strengths include the permanent stratification of Red Pond and the timing of stratified and isothermal periods in Bear Lake (Fig. 3 for subset; see Figs. S10 and S11 for all years). Out of the 1000 total simulations, all parameter sets reproduce the approximate timing of ice-on, so we reject none based on that calibration criteria. We select the 30 best-performing (lowest RMSE) water temperature profile simulations for each lake. The RMSE ensemble average was 1.55 °C for Bear Lake and 0.66 °C for Red Pond (Table 3). The most sensitive parameters for simulating water temperature profiles in these lakes are the light extinction and neutral drag coefficients, which parameterize water clarity and evaporation, respectively (Morrill et al., 2019). The calibrated range of the light extinction coefficient is 2.73-3.25 m^{-1} (Z_{SD} = 0.48-0.58 m) for Red Pond and 0.57-0.73 m^{-1} (Z_{SD} = 2.15-2.75 m) for Bear Lake, reflecting the high turbidity of these lakes. The environment submodel defines a static light extinction coefficient but allowing seasonal or yearly flexibility in this parameter could be useful for improving model fit further, given that water clarity can vary over time and this could be reflected in multi-year observational datasets used for calibration (Fig. S7). The Red Pond simulations are additionally sensitive to the albedo of snow, reflecting how Red Pond's smaller surface area may be more responsive to changes in surface energy than Bear Lake. Insensitive parameters were sampled approximately uniformly across their prescribed ranges in the calibrated 30-member ensemble (Figs. S12).

https://doi.org/10.5194/egusphere-2026-2322
Preprint. Discussion started: 20 May 2026
© Author(s) 2026. CC BY 4.0 License.

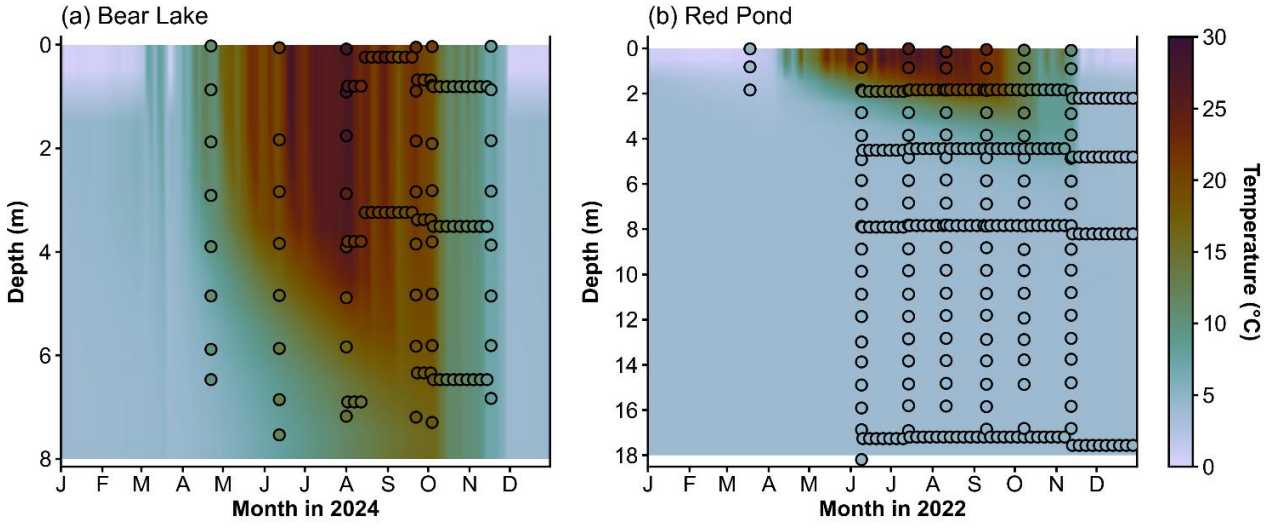

Figure 3: Results of environment submodel calibration to observed water temperature profiles from (a) Bear Lake and (b) Red Pond. Colors are modeled ensemble means for each day and depths. Dots are observations, colored by observed water temperature. Note that we performed calibrations on the full multi-year datasets (shown in Supplement) and only show a subset here. For dense periods of daily observations, we plot every 5th measurement but calibrated to all measurements. Colormap from Crameri et al. (2020).

Table 3: Environment submodel performance for water temperature and δ^2H profiles, surface, and bottom. RMSE and bias scores are the average results from each calibrated 30-member ensemble. Scores for the profiles are shown in bold text.

Variable	RMSE (bias)
Bear Lake	
Water temperature profiles (°C)	**1.55 (-0.25)**
Surface water temperature (°C)	0.97 (-0.58)
Bottom water temperature (°C)	1.72 (-0.95)
Water δ^2H profiles (‰ VSMOW)	**11.25 (-0.94)**
Surface water δ^2H value (‰ VSMOW)	13.54 (3.15)
Bottom δ^2H value (‰ VSMOW)	6.57 (-2.03)
Red Pond	
Water temperature profiles (°C)	**0.66 (-0.41)**
Surface water temperature (°C)	1.38 (-0.56)
Bottom water temperature (°C)	0.71 (-0.71)
Water δ^2H profiles (‰ VSMOW)	**4.25 (-0.37)**
Surface water δ^2H value (‰ VSMOW)	6.94 (1.40)
Bottom δ^2H value (‰ VSMOW)	1.96 (-0.79)

https://doi.org/10.5194/egusphere-2026-2322
Preprint. Discussion started: 20 May 2026
© Author(s) 2026. CC BY 4.0 License.

Using our runoff module and framework to prescribe precipitation and runoff isotope values and drive the environment submodel, seasonal variability in observed lake water δ^2H profiles at Bear Lake and Red Pond is well represented by the simulations (Fig. 4c; see S13 and S14 for other depths). Our simulations reproduce ^2H-enriched summer lake water compared to winter δ^2H values, reflecting the seasonal trends of precipitation isotopic composition characteristic of western New York (Fig. 4a; Corcoran et al., 2019). The 30 best-performing lake water δ^2H profile simulations for each lake result in RMSE ensemble averages of 11.25 ‰ for Bear Lake and 4.25 ‰ for Red Pond, with most misfit coming from the surface/epilimnion (Table 3; Figures S13 and S14). Because water temperature impacts isotopic fractionation during evaporation, simulated lake water δ^2H values are sensitive to thermal parameters. Other sensitive parameters are the fraction and water vapor isotope value of the atmospheric boundary layer advected from adjacent land and runoff-to-precipitation ratios (Table 1). The best-performing simulations for both lakes use an air mass consisting of more than 50% advected air ($f > 0.50$). This suggests that the water vapor in the air mass above the lake when our observations were collected was mostly derived from advected air rather than from evaporating lake water.

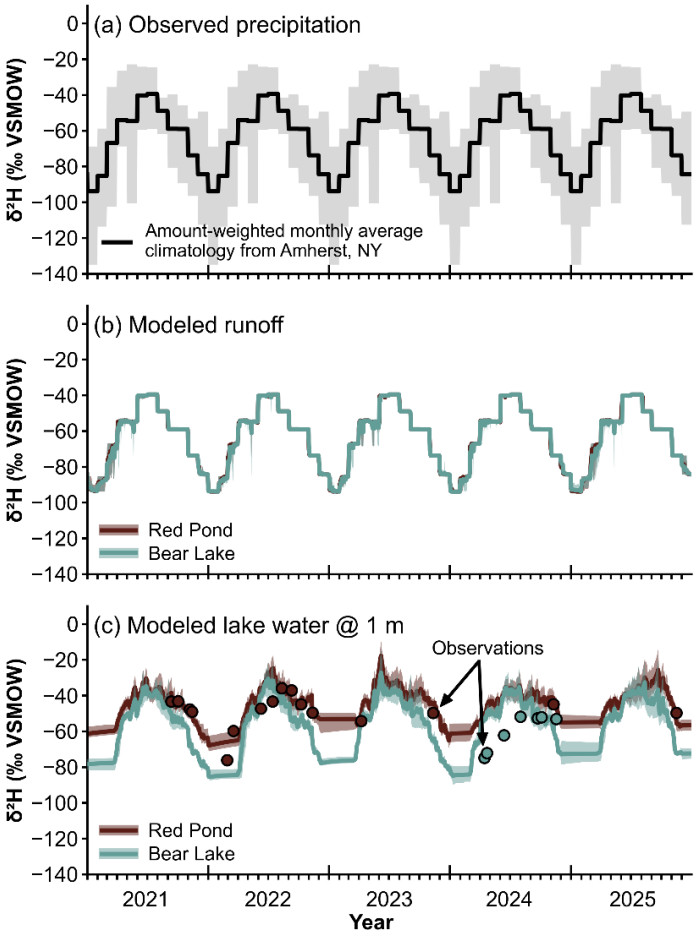

Figure 4. Inputs and outputs for simulating lake water δ^2H values using the environment submodel. Our simulations cover years 1995-2025, but we only show 2021-2025 here where observations overlap with simulations. (a) Amount-weighted monthly average precipitation δ^2H climatology based on observations from Amherst, New York that forced the runoff module and environment submodel. Gray shading shows the 5th to 95th percentiles of the amount-weighted monthly observations across the entire dataset. (b) Modeled runoff δ^2H values calculated using the runoff module. (c) Results of environment submodel calibration to observed lake water δ^2H profiles. Lines are modeled values at 1 m depth. Dots are observations. In (b) and (c), thick lines are modeled ensemble means and shading shows the 5-95th percentile of the ensemble.

https://doi.org/10.5194/egusphere-2026-2322
Preprint. Discussion started: 20 May 2026
© Author(s) 2026. CC BY 4.0 License.

One source of the mismatch between observed and simulated lake water δ^2H profiles (Fig. 4c) could be parameter uncertainty. To investigate this, we evaluate average ice-free season epilimnion δ^2H values (average of surface to 3 m depth) for all 30 modeled years across the 1000 lake water δ^2H profile simulations for both lakes (Fig. 5). We define the ice-free season as days when the fraction of ice on the lake is zero. We focus on the ice-free season because that is the window most lake sediment proxies reflect (Castañeda and Schouten, 2011). The range of lake water δ^2H values for the 1000 simulations is 29 ‰ for Bear Lake and 64 ‰ for Red Pond. For both lakes, runoff parameters have little impact on simulated lake water δ^2H values. Thermal and isotope parameters drive the spread in simulated values for Red Pond. This makes sense because those parameters impact evaporation amount and isotopic fractionation during evaporation, which strongly influence Red Pond's isotopic composition as a closed-basin lake. Because Bear Lake is hydrologically open and receives substantial runoff due to its large catchment, its isotopic composition is less strongly influenced by thermal and isotope parameters. However, Bear Lake does have large variability in simulated lake water δ^2H values, which means the model forcing may matter more than parameter values for simulating that lake.

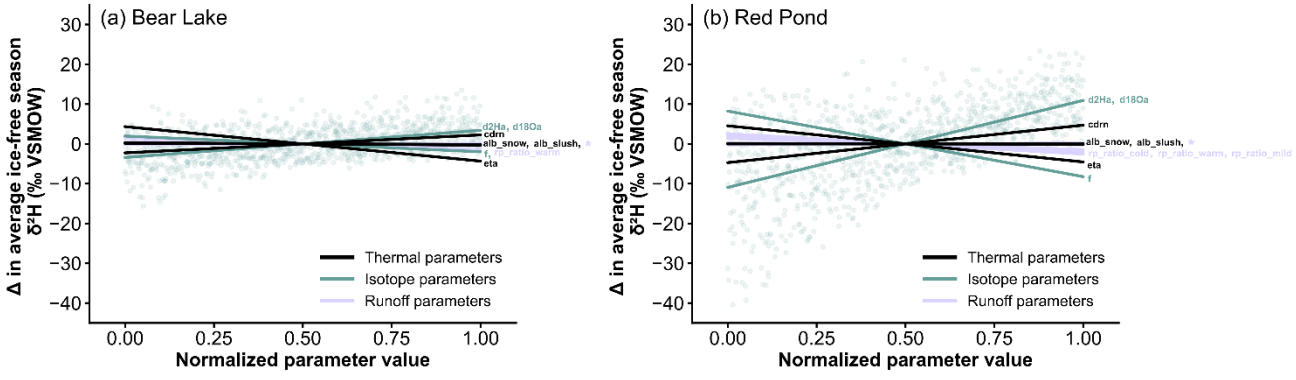

Figure 5. Summary of 1000 lake water δ^2H profile simulations with different parameters sampled using Latin Hypercube for (a) Bear Lake and (b) Red Pond. Lines are colored by parameter category and represent lines of best fit through the distribution of each parameter across the sampled range for the average ice-free season δ^2H values of the epilimnion (surface to 3 m depth) for all 30 years. Parameter values are normalized so they can plot on the same axis (see Table 1 for actual values), and lake water δ^2H values are displayed as anomalies from the parameter values at 0.50. Annotations at the end of each line identify individual parameters, where * indicates all runoff parameters not listed. Blue points show an example of the parameter distribution for one parameter: the δ^2H value of the atmospheric boundary layer water vapor.

Another reason for errors between the observations and simulations could be due to uncertainty within the precipitation isotope forcing. We force the runoff module and environment submodel with an amount-weighted monthly average climatology from Amherst, New York, which is approximately 85 km northeast of our study sites (Fig. 1a). Therefore, the true isotope values, timing, and amount of rainfall that fell onto the lakes when our observations were collected could be

https://doi.org/10.5194/egusphere-2026-2322
Preprint. Discussion started: 20 May 2026
© Author(s) 2026. CC BY 4.0 License.

different than the forcing. Further, using a climatology simplifies the system, but allows for simulations beyond an often short (i.e., a few years) observational window (IAEA/WMO, 2015). Because our simulations reproduce the approximate magnitude and seasonal timing of our lake water δ^2H observations, we view them as useful representations of the two lake systems on seasonal and longer timescales.

We recognize that the precipitation isotope forcing has larger uncertainties than other variables that force the lake model (e.g. air temperature or shortwave radiation). Quality meteorological inputs are critical given that the accuracy of the environment submodel and application of the PSM to interpret lake sediment archives depends on the accuracy of the calibration to the modern lake system. To address this, we test different versions of the precipitation isotope climatology we use to force the environment submodel to quantify how uncertainty might influence simulated lake water isotope values. Using the 30-member ensemble from our calibration (Fig. 4c) forced with the amount-weighted monthly average climatology, we complete two experiments using different forcings for each lake: the 5th percentile climatology and 95th percentile climatology of the amount-weighted monthly averages (as in Fig. 4a). Then, we examine the change in modeled epilimnion δ^2H values (average of surface to 3 m depth). We show that both the Bear Lake and Red Pond simulated ice-free average lake water δ^2H values are sensitive to the precipitation isotope forcing (Fig. 6). Using the 5th percentile climatology, the median ice-free average lake water δ^2H values for Bear Lake and Red Pond are 22.22 ‰ and 17.90 ‰ depleted relative to simulations forced using the average climatology. Using the 95th percentile climatology, the median ice-free average lake water δ^2H values for Bear Lake and Red Pond are 17.91 ‰ and 14.78 ‰ enriched relative to simulations forced using the average climatology.

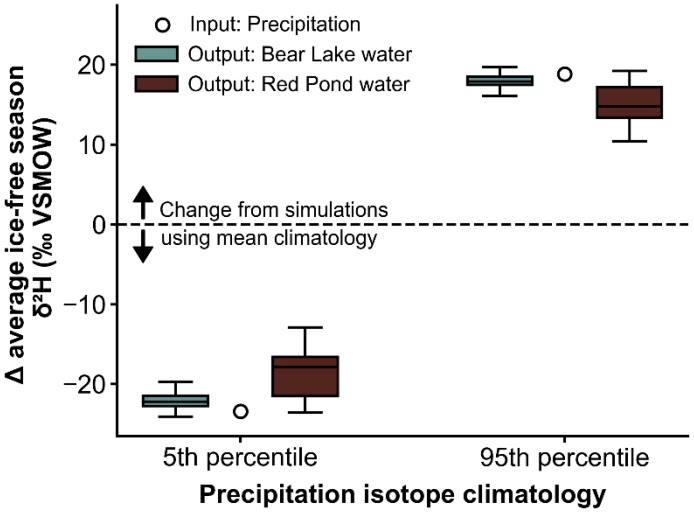

Figure 6. We tested the sensitivity of modeled lake water δ^2H values when the environment submodel is forced with different precipitation isotope climatologies. Open black circles show the ice-free season (April-November) average of either the monthly amount-weighted 5th or 95th percentile climatology (see Figure 4a). Box plots show average ice-free season lake water δ^2H values of the epilimnion (surface to 3 m depth) across all 30 years for each of the 30 ensemble members under the different forcings. For each box plot, horizontal lines show the median average ice-free lake water δ^2H value across the ensemble, the box indicates the 25th to 75th quartile range, and the whiskers display the minimum and maximum values.

https://doi.org/10.5194/egusphere-2026-2322
Preprint. Discussion started: 20 May 2026
© Author(s) 2026. CC BY 4.0 License.

4.3 Effects of limited calibration data on environment submodel performance

When only a single lake water temperature profile observation is available, the performance of the Red Pond and Bear Lake environment submodels remain reliable and robust. However, performance varied widely by season, with the best-performing environment submodel ensembles resulting from calibration on lake water temperature profiles collected during the warm, ice-free period dates (Fig. 7). The 30-member ensemble average RMSE on any given date in our dataset ranged from 0.67 °C to 6.96 °C for Red Pond and 1.54 °C to 8.31 °C for Bear Lake. Dates with the highest ensemble average RMSE values, and the most ensemble spread, occur with environment submodel calibration to water temperature profiles that were collected when the lakes were ice-covered. However, the under-ice RMSE scores are not consistent among years (at Red Pond), perhaps due to differences in ice cover conditions (e.g. ice thickness, ice break-up and refreeze, etc). We only have one under-ice water temperature profile from Bear Lake, but it also has the highest RMSE of any date tested from that dataset. We identify the warm, ice-free period (in these lakes, ~day of year 125-265, or early May to late September) as the most informative sampling window for simulation of both Red Pond and Bear Lake water temperature profiles. On these dates, ensemble average RMSE values are almost equivalent as calibration to all water temperature observations (Table 3), and RMSE values are consistent across sampling years. The RMSE for water temperature profiles during this window span 0.67 °C to 1.20 °C for Red Pond and 1.54 °C to 2.04 °C for Bear Lake. These RMSE scores are comparable to performance metrics from other studies applying this model (Almeida et al., 2022; Martynov et al., 2010; Perroud et al., 2009; Sae-Lim et al., 2025) and other lake water temperature models (Jia et al., 2021; Ladwig et al., 2024; Martynov et al., 2010; Read et al., 2019).

https://doi.org/10.5194/egusphere-2026-2322
Preprint. Discussion started: 20 May 2026
© Author(s) 2026. CC BY 4.0 License.

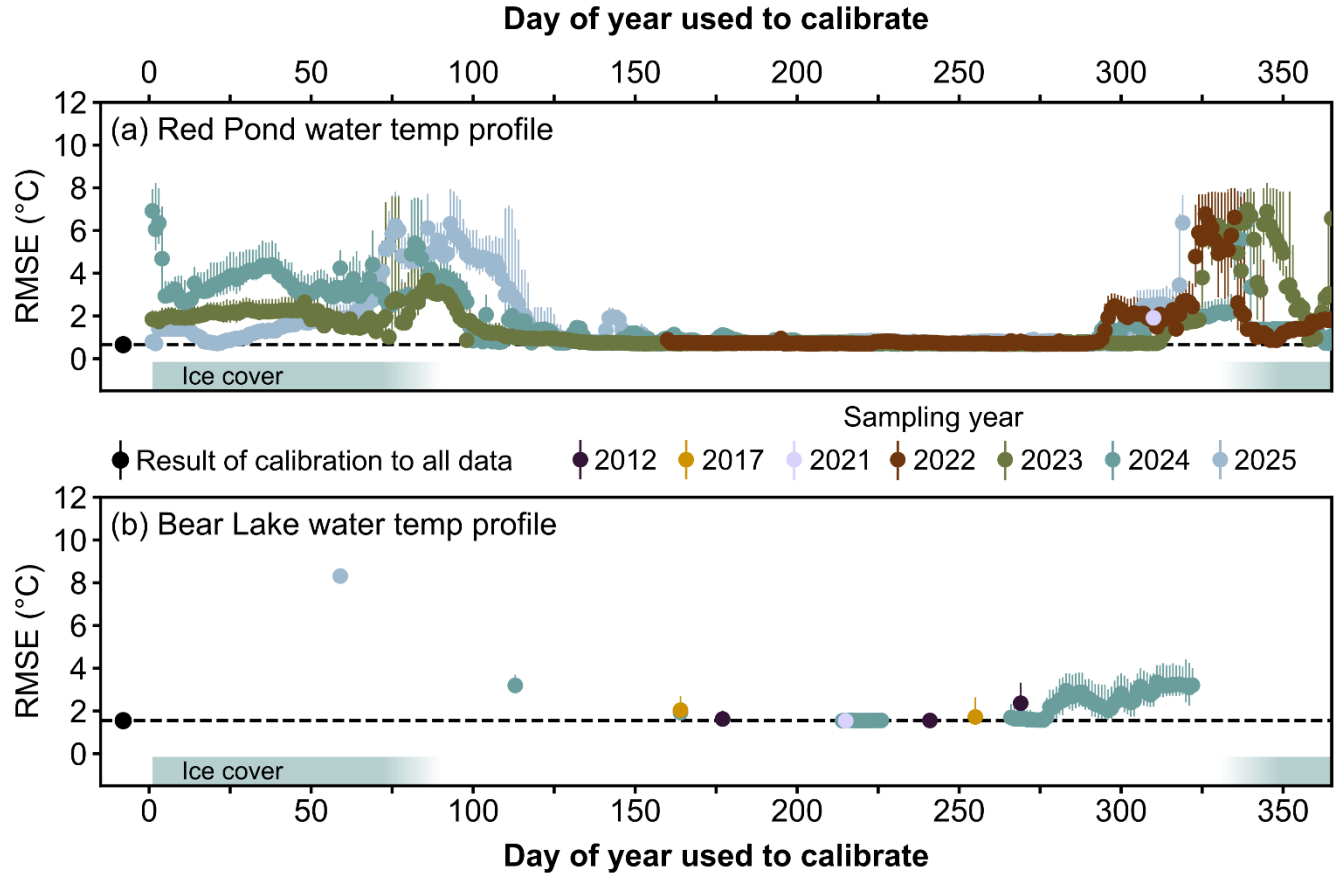

Figure 7. Effect of environment submodel calibration to an observed water temperature profile from one date as measured by root-mean-square error (RMSE) for (a) Red Pond and (b) Bear Lake. We calibrated each date by choosing the 30 best-performing simulations from 1000 total simulations. RMSE values reflect model performance over the validation period (all remaining observations). Dots show the ensemble average RMSE and bars show the 5th and 95th percentile RMSE of the ensemble, colored by the year the profile was sampled. We show the result of environment submodel calibration to all water temperature observations (as in Figure 3) for each lake as a black dot. Colormap from Crameri et al. (2020).

Environment submodel calibration to lake water δ^2H profile observations from one date have a less clear trend regarding which dates are most informative. Generally, summer dates have the lowest RMSE and show the most agreement among ensemble members (Fig. 8). The 30-member ensemble average RMSE for any given date in our dataset ranged from 4.31 to 8.77 ‰ for Red Pond and 12.77 to 15.47 ‰ for Bear Lake. From the Red Pond experiment, most dates result in an RMSE score similar to calibration using all water δ^2H observations (Table 3), with dates under-ice or within a few weeks after ice-off being the worst-performing. For Bear Lake, calibration to spring and summer dates resulted in the lowest RMSE scores.

https://doi.org/10.5194/egusphere-2026-2322
Preprint. Discussion started: 20 May 2026
© Author(s) 2026. CC BY 4.0 License.

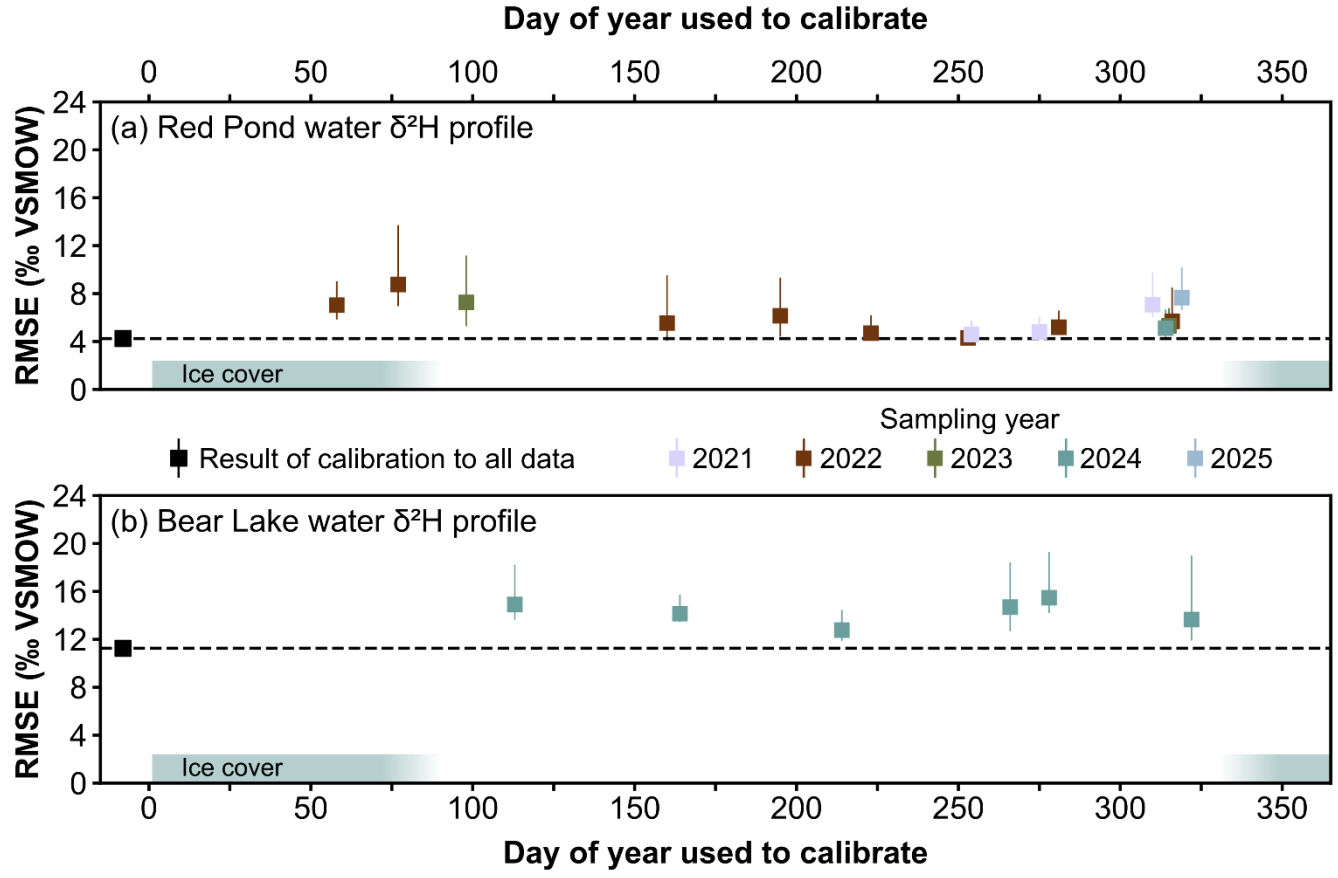

Figure 8. Effect of environment submodel calibration to an observed water δ^2H profile from one date as measured by root-mean-square error (RMSE) for (a) Red Pond and (b) Bear Lake. We calibrated each date by choosing the 30 best-performing simulations from 1000 total simulations. RMSE values reflect model performance over the validation period (all remaining observations). Squares show the ensemble average RMSE and bars show the 5th and 95th percentile RMSE of the ensemble, colored by the year the profile was sampled. We show the result of environment submodel calibration to all water δ^2H observations (as in Figure 4c) for each lake as a black square. Colormap from Crameri et al. (2020).

https://doi.org/10.5194/egusphere-2026-2322
Preprint. Discussion started: 20 May 2026
© Author(s) 2026. CC BY 4.0 License.

5 Discussion

PSMs support mechanistic interpretations of paleoclimate data from lake sediments that incorporate uncertainty. However, two obstacles hinder their wider use: (1) Lack of long-term, continuous precipitation isotope observations and a built-in catchment model make simulating lake water isotope values challenging, and (2) observational datasets for environment submodel calibration are often sparse. Most lakes are not well-monitored (Stanley et al., 2019), especially remote sites where few observations can be collected and sites from which paleoclimate datasets have been generated but cannot be easily revisited. We integrate a runoff-isotope module into the PSM and craft guidelines for the most useful observations for environment submodel calibration to help overcome these obstacles.

We show that sparse observational datasets of lake water temperature and δ^2H profiles can result in reliable and robust environment submodel calibration for proxy system modeling applications. We find that environment submodel calibration to a single profile observation measured during the warm, ice-free season, when the lakes are most stable, results in the selection of parameter sets that generalize the best to unseen data from other years and depths. We show that performance measured by RMSE in the validation period for simulated water temperature profiles of two mid-latitude lakes calibrated to a single summer observed profile is less than 2 °C, which is small relative to large uncertainties in proxy calibrations. The RMSE of the validation period for simulated water δ^2H profiles results in larger errors compared to water temperature profiles, even when calibrated to many ($n > 6$) profile observations. We attribute these errors to uncertainties within the precipitation isotope forcing (Fig. 6) rather than lake-specific or runoff parameter uncertainty. However, observations measured on summer dates seem to be the most informative.

Several factors explain why water temperature profiles from the warm, ice-free season are the most informative for environment submodel calibration. In this model, the thermal parameters with the most influence on water temperatures (light extinction and neutral drag coefficients) are most sensitive to the ice-free season. The light extinction coefficient controls how deeply solar radiation can penetrate into the water column, and thus the strength of stratification. Because parameters are constant for the entire simulation, summer water temperature profiles capture the period of maximum summer stratification, thus are most informative for constraining that uncertain parameter. The neutral drag coefficient describes surface roughness, which impacts wind-driven mixing and evaporation, and therefore becomes unimportant when the lake is ice-covered. In Figure 7, calibration for under-ice dates has a large spread in RMSE scores among the 30 ensemble members, illustrating the disagreement among parameter sets due to observations not sufficiently constraining parameter values. The few weeks before ice-on and after ice-off are also unsatisfactory calibration targets. When the lake is isothermal (or in the case of Red Pond, the metalimnion is isothermal), the thermal stability is weaker, and thus observations from those dates are also less informative.

https://doi.org/10.5194/egusphere-2026-2322
Preprint. Discussion started: 20 May 2026
© Author(s) 2026. CC BY 4.0 License.

Environment submodel calibration to water δ^2H profiles is more complex and controlled by thermal parameters as well as runoff and isotope-specific parameters, which means that observational datasets must reflect several processes. Unlike the water temperature profile experiment, the water isotope experiment for Red Pond and Bear Lake shows different trends in which dates are most informative for environment submodel calibration. This likely stems from the stability of Red Pond compared to Bear Lake, and the lakes' contrasting hydrologic characteristics. As shown in Fig. 6, Bear Lake water δ^2H values closely track precipitation δ^2H values, which is a similar result as the simulation of open-basin lakes in other lake models (Jones et al., 2016). Meanwhile, closed-basin lakes like Red Pond are dominated by an evaporation signal, where short-term variability in precipitation δ^2H forcing has a smaller impact on simulated lake water δ^2H values (Hostetler and Benson, 1994; Jones et al., 2016; Steinman et al., 2010). Because Red Pond's morphology and hydrology make the lake less sensitive to precipitation δ^2H forcing, a single lake water δ^2H profile from the ice-free season can constrain environment submodel parameters that generalize well to other years and depths. While this is the case for Red Pond, other closed-basin lakes may be more sensitive to precipitation δ^2H forcing depending on their outseepage and morphometry (Steinman et al., 2010). Outseepage can provide a pathway for a closed-basin lake to lose water other than evaporation. For example, if the rate of water outflow through seepage is high and the lake's surface area is small relative to its volume, evaporation might not buffer lake water δ^2H values in the same way. In any case, the precipitation δ^2H forcing should be chosen carefully, but especially when using the environment submodel to simulate open-basin lakes with large catchments that are sensitive to inputs.

Essential to better modeling of lake water δ^2H profiles is precipitation isotope monitoring (Birkel et al., 2025; Jones et al., 2016), which is useful for lake proxy system modeling and other paleoclimate applications. Lake models that simulate water isotopes seem to perform best when forced with local, daily observations rather than a climatology (Hostetler and Benson, 1994; Jones et al., 2016; Steinman et al., 2010), but using daily observations limits the simulation to the window when observations were collected. To improve our simulations of lake water isotope values using the runoff module integrated with the environment submodel, the precipitation isotope forcing could be parameterized to help constrain and characterize uncertainty within the forcing and allow for year-to-year variability.

We aimed to provide environment submodel calibration and sampling guidelines that apply to many different lakes and support our guidelines with results from two lakes with contrasting morphometries, mixing regimes, and hydrology. Our study lakes represent two endmember systems with respect to water temperature and δ^2H profiles. However, we acknowledge that both of our study sites are in the same region and experience the same climate. Climate controls the length of the ice-free season, and thus the strength of stratification and amount of evaporation, runoff, and precipitation entering the lake. Therefore, the most informative sampling window will likely change depending on lake location. For example, Arctic lakes have a shorter ice-free season than lakes in the mid-latitudes (Arp et al., 2010). This would shorten the window for when most informative water temperature and isotope profiles could be collected. Additionally, the sampling guidelines we

https://doi.org/10.5194/egusphere-2026-2322
Preprint. Discussion started: 20 May 2026
© Author(s) 2026. CC BY 4.0 License.

describe most likely only apply to temperate lakes. Lakes that mix more frequently, such as shallow polymictic lakes found in the tropics and subtropics (e.g. Mosquera et al., 2025) or lakes that are permanently ice-covered, may have different windows where observations are most informative. Despite this, the tools, runoff module, and calibration framework we describe are adaptable for simulating any lake system and therefore can be used to assess performance in other climates.

6 Conclusion

In this paper, we addressed two obstacles hindering the broad use of PSMs for interpretation of lake sediment archives. We developed and tested a runoff-isotope module, which aids the PSM's environment submodel in simulating lake water isotopes. Using a parallel processing framework to rapidly run the environment submodel and thoroughly sample the parameter space, we reproduced lake water temperature and δ^2H profiles at two mid-latitude lakes with contrasting characteristics. Through model experiments, we showed that sparse observational data does not necessarily hinder environment submodel performance, and crafted guidelines to target the most informative temporal windows to collect observations for calibration, even when time, resources, or site location limit field season duration. These contributions will advance proxy system modeling by reducing time spent on model set-up and calibration. These tools and framework are a step towards unlocking the vast global database of lake sediment paleoclimate time series as climate model validation targets able to improve our ability to predict and prepare for a warmer world.

Code and data availability

Code for the version of the environment submodel and runoff module described in this paper are available on Zenodo (https://doi.org/10.5281/zenodo.20124941; Topness et al., 2026a), along with a detailed user tutorial that contains step-by-step instructions on running the parallel processing framework and example calibration workbooks in Python. Model inputs and outputs are archived in a separate Zenodo repository (https://doi.org/10.5281/zenodo.19775686, Topness et al., 2026d) that includes the code and data required to reproduce our results and figures. The current version of the model is available on GitHub (https://github.com/rgtopness/lake-psm-calibration/, last access: 11 May 2026). Observations collected from Bear Lake and Red Pond are publicly available on Hydroshare (Topness et al., 2026b, c), together with both raw and post-processed datasets, a user guide, and the code used to process the data.

https://doi.org/10.5194/egusphere-2026-2322
Preprint. Discussion started: 20 May 2026
© Author(s) 2026. CC BY 4.0 License.

Author contributions

RGT and EKT conceptualized the study. MF updated the treatment of lake water isotopes from the original model code (https://github.com/carriemorrill/lake-model/tree/lake-model-isotopes). GAO developed and wrote the code for the parallel processing framework. RGT developed the code for the runoff module, adapted the parallel processing code for this work, and integrated the runoff module into the framework. All authors helped collect field observations. RGT ran the model simulations and executed the experiments with supervision from EKT. RGT wrote the paper with input from all authors.

Competing interests

The authors declare that they have no conflict of interest.

Disclaimer

Copernicus Publications remains neutral with regard to jurisdictional claims made in the text, published maps, institutional affiliations, or any other geographical representation in this paper. While Copernicus Publications makes every effort to include appropriate place names, the final responsibility lies with the authors. Views expressed in the text are those of the authors and do not necessarily reflect the views of the publisher.

Acknowledgements

We thank Sudip Acharya, Diana Aga, Haben Berhe, Niyat Berhe, the Briner boys, Eriyon Cowles, Andrew Cuzzacrea, Katie Eaman, Emily Earl, Fiona Ellsworth, Harleena Franklin, Sean Grasing, Devon Gorbey, Brandon Graham, Hannah Holtzman, Leone Jacobson, Corey Krabbenhoft, Nancy Leon, Kurt Lindberg, Samuel Mark, Hayley Martinez, Grace Maxson, Nicholas Ohnmeiss, Travis Parsons, Karlee Prince, Justus Rodriguez, Abigail Stressinger, George Thomas, Joe Tulenko, Caleb Walcott, and Liza Wilson for help in the field. Thanks to Nancy Leon, Haben Berhe, Trevor Krabbenhoft, and Katie Patchett for logistical and lab support. Special thanks to Bob, Joan, Bob Jr., Jamie, Kathy, and Greg Gebhard, Tom Bohall (Red Pond), Sidney Potmesil, and the New York State Department of Environmental Conservation (Bear Lake) for field access and support.

Financial support

This research has been supported by the National Science Foundation (AGS-2044616) and the Geological Society of America (Graduate Student Research Grant and Continental Scientific Drilling Division Research Grant).

https://doi.org/10.5194/egusphere-2026-2322
Preprint. Discussion started: 20 May 2026
© Author(s) 2026. CC BY 4.0 License.

Review statement

The review statement will be added by Copernicus Publications listing the handling editor as well as all contributing referees according to their status anonymous or identified.

References

Acharya, S., Cluett, A. A., Grogan, A. L., Briner, J. P., Castañeda, I. S., and Thomas, E. K.: Holocene temperatures in southwestern Greenland controlled by topography, ice sheet proximity and oceanic conditions, https://doi.org/10.5194/egusphere-2025-3113, 31 July 2025.

Almeida, M. C., Shevchuk, Y., Kirillin, G., Soares, P. M. M., Cardoso, R. M., Matos, J. P., Rebelo, R. M., Rodrigues, A. C., and Coelho, P. S.: Modeling reservoir surface temperatures for regional and global climate models: a multi-model study on the inflow and level variation effects, Geosci. Model Dev., 15, 173–197, https://doi.org/10.5194/gmd-15-173-2022, 2022.

Arp, C. D., Jones, B. M., Whitman, M., Larsen, A., and Urban, F. E.: Lake Temperature and Ice Cover Regimes in the Alaskan Subarctic and Arctic: Integrated Monitoring, Remote Sensing, and Modeling1, JAWRA J. Am. Water Resour. Assoc., 46, 777–791, https://doi.org/10.1111/j.1752-1688.2010.00451.x, 2010.

Birkel, C., Miller, J., Watson, A., Anh Trinh, D., Durán-Quesada, A. M., Sánchez-Murillo, R., Soulsby, C., Terzer-Wassmuth, S., Tetzlaff, D., Uhlenbrook, S., Vystavna, Y., and Yoshimura, K.: Demystifying the art of isotope-enabled hydrological and climate modelling, Sci. Total Environ., 959, 178242, https://doi.org/10.1016/j.scitotenv.2024.178242, 2025.

Bigham Stephens, D. L., Carlson, R. E., Horsburgh, C. A., Hoyer, M. V., Bachmann, R. W., and Canfield, D. E.: Regional distribution of Secchi disk transparency in waters of the United States, Lake and Reservoir Management, 31, 55–63, https://doi.org/10.1080/10402381.2014.1001539, 2015.

Bowen, G. J., Wassenaar, L. I., and Hobson, K. A.: Global application of stable hydrogen and oxygen isotopes to wildlife forensics, Oecologia, 143, 337–348, https://doi.org/10.1007/s00442-004-1813-y, 2005.

Bowen, G. J.: The Online Isotopes in Precipitation Calculator, version 3.1., http://www.waterisotopes.org, 2017.

Braconnot, P., Harrison, S. P., Kageyama, M., Bartlein, P. J., Masson-Delmotte, V., Abe-Ouchi, A., Otto-Bliesner, B., and Zhao, Y.: Evaluation of climate models using palaeoclimatic data, Nat. Clim. Change, 2, 417–424, https://doi.org/10.1038/nclimate1456, 2012.

Castañeda, I. S. and Schouten, S.: A review of molecular organic proxies for examining modern and ancient lacustrine environments, Quat. Sci. Rev., 30, 2851–2891, https://doi.org/10.1016/j.quascirev.2011.07.009, 2011.

Cluett, A.A.: Investigating late Quaternary temperature and precipitation dynamics on Greenland using precipitation isotope and organic geochemical proxies, Ph.D. thesis, University at Buffalo, Buffalo, New York, 2021.

https://doi.org/10.5194/egusphere-2026-2322
Preprint. Discussion started: 20 May 2026
© Author(s) 2026. CC BY 4.0 License.

Cluett, A. A., Thomas, E. K., McKay, N. P., Cowling, O. C., Castañeda, I. S., and Morrill, C.: Lake Dynamics Modulate the Air Temperature Variability Recorded by Sedimentary Aquatic Biomarkers: A Holocene Case Study From Western Greenland, J. Geophys. Res. Biogeosciences, 128, e2022JG007106, https://doi.org/10.1029/2022JG007106, 2023.

Corcoran, M. C., Thomas, E. K., and Boutt, D. F.: Event-Based Precipitation Isotopes in the Laurentian Great Lakes Region Reveal Spatiotemporal Patterns in Moisture Recycling, Journal of Geophysical Research: Atmospheres, 124, 5463–5478, https://doi.org/10.1029/2018JD029545, 2019.

Corcoran, M. C., Thomas, E. K., and Morrill, C.: Using a Paired Chironomid δ18O and Aquatic Leaf Wax δ2H Approach to Reconstruct Seasonality on Western Greenland During the Holocene, Paleoceanography and Paleoclimatology, 36, e2020PA004169, https://doi.org/10.1029/2020PA004169, 2021.

Crameri, F., Shephard, G. E., and Heron, P. J.: The misuse of colour in science communication, Nat Commun, 11, 5444, https://doi.org/10.1038/s41467-020-19160-7, 2020.

D. N. Moriasi, J. G. Arnold, M. W. Van Liew, R. L. Bingner, R. D. Harmel, and T. L. Veith: Model Evaluation Guidelines for Systematic Quantification of Accuracy in Watershed Simulations, Trans. ASABE, 50, 885–900, https://doi.org/10.13031/2013.23153, 2007.

Dee, S., Bailey, A., Conroy, J. L., Atwood, A., Stevenson, S., Nusbaumer, J., and Noone, D.: Water isotopes, climate variability, and the hydrological cycle: recent advances and new frontiers, Environ. Res. Clim., 2, 022002, https://doi.org/10.1088/2752-5295/accbe1, 2023.

Dee, S. G., Russell, J. M., Morrill, C., Chen, Z., and Neary, A.: PRYSM v2.0: A Proxy System Model for Lacustrine Archives, Paleoceanogr. Paleoclimatology, 33, 1250–1269, https://doi.org/10.1029/2018PA003413, 2018.

Dee, S. G., Morrill, C., Kim, S. H., and Russell, J. M.: Hot Air, Hot Lakes, or Both? Exploring Mid-Holocene African Temperatures Using Proxy System Modeling, J. Geophys. Res. Atmospheres, 126, e2020JD033269, https://doi.org/10.1029/2020JD033269, 2021.

Evans, M. N., Tolwinski-Ward, S. E., Thompson, D. M., and Anchukaitis, K. J.: Applications of proxy system modeling in high resolution paleoclimatology, Quat. Sci. Rev., 76, 16–28, https://doi.org/10.1016/j.quascirev.2013.05.024, 2013.

Guiot, J., Torre, F., Jolly, D., Peyron, O., Boreux, J. J., and Cheddadi, R.: Inverse vegetation modeling by Monte Carlo sampling to reconstruct palaeoclimates under changed precipitation seasonality and CO2 conditions: application to glacial climate in Mediterranean region, Ecological Modelling, 127, 119–140, https://doi.org/10.1016/S0304-3800(99)00219-7, 2000.

Guiot, J., Wu, H. B., Garreta, V., Hatté, C., and Magny, M.: A few prospective ideas on climate reconstruction: from a statistical single proxy approach towards a multi-proxy and dynamical approach, Clim. Past, 5, 571–583, https://doi.org/10.5194/cp-5-571-2009, 2009.

Haslett, J., Whiley, M., Bhattacharya, S., Salter-Townshend, M., Wilson, S. P., Allen, J. R. M., Huntley, B., and Mitchell, F. J. G.: Bayesian Palaeoclimate Reconstruction, Journal of the Royal Statistical Society Series A: Statistics in Society, 169, 395–438, https://doi.org/10.1111/j.1467-985X.2006.00429.x, 2006.

https://doi.org/10.5194/egusphere-2026-2322
Preprint. Discussion started: 20 May 2026
© Author(s) 2026. CC BY 4.0 License.

Hersbach, H., Bell, B., Berrisford, P., Hirahara, S., Horányi, A., Muñoz-Sabater, J., Nicolas, J., Peubey, C., Radu, R., Schepers, D., Simmons, A., Soci, C., Abdalla, S., Abellan, X., Balsamo, G., Bechtold, P., Biavati, G., Bidlot, J., Bonavita, M., De Chiara, G., Dahlgren, P., Dee, D., Diamantakis, M., Dragani, R., Flemming, J., Forbes, R., Fuentes, M., Geer, A., Haimberger, L., Healy, S., Hogan, R. J., Hólm, E., Janisková, M., Keeley, S., Laloyaux, P., Lopez, P., Lupu, C., Radnoti, G., De Rosnay, P., Rozum, I., Vamborg, F., Villaume, S., and Thépaut, J.: The ERA5 global reanalysis, Q. J. R. Meteorol. Soc., 146, 1999–2049, https://doi.org/10.1002/qj.3803, 2020.

Hersbach, H., Bell, B., Berrisford, P., Biavati, G., Horányi, A., Muñoz Sabater, J., Nicolas, J., Peubey, C., Radu, R., Rozum, I., Schepers, D., Simmons, A., Soci, C., Dee, D., Thépaut, J-N.: ERA5 hourly data on single levels from 1940 to present, Copernicus Climate Change Service (C3S) Climate Data Store (CDS), [data set], https://doi.org/10.24381/cds.adbb2d47, 2023.

Holtzman, H., Thomas, E. K., Erb, M., Marshall, L., Castañeda, I. S., Kaufman, D., McKay, N. P., and Melles, M.: Early Holocene Atmospheric Circulation Changes Over Northern Europe Based on Isotopic and Biomarker Evidence From Kola Peninsula, Paleoceanogr. Paleoclimatology, 40, e2024PA005076, https://doi.org/10.1029/2024PA005076, 2025.

Hostetler, S. and Benson, L. V.: Paleoclimatic implications of the high stand of Lake Lahontan derived from models of evaporation and lake level, Clim. Dyn., 4, 207–217, https://doi.org/10.1007/BF00209522, 1990.

Hostetler, S. W.: Simulation of lake ice and its effect on the late-Pleistocene evaporation rate of Lake Lahontan, Clim. Dyn., 6, 43–48, https://doi.org/10.1007/BF00210581, 1991.

Hostetler, S. W. and Bartlein, P. J.: Simulation of lake evaporation with application to modeling lake level variations of Harney-Malheur Lake, Oregon, Water Resour. Res., 26, 2603–2612, https://doi.org/10.1029/WR026i010p02603, 1990.

Hostetler, S. W. and Benson, L. V.: Stable isotopes of oxygen and hydrogen in the Truckee River–Pyramid Lake surface-water system. 2. A predictive model of δ18O and δ2H in Pyramid Lake, Limnol. Oceanogr., 39, 356–364, https://doi.org/10.4319/lo.1994.39.2.0356, 1994.

Hrycik, A. R., Isles, P. D. F., Pierson, D. C., and Stockwell, J. D.: Winter/Spring Runoff Is Earlier, More Protracted, and Increasing in Volume in the Laurentian Great Lakes Basin, Water Resour. Res., 60, e2023WR035773, https://doi.org/10.1029/2023WR035773, 2024.

IAEA/WMO, Global Network of Isotopes in Precipitation, GNIP Database [data set], https://nucleus.iaea.org/wiser, 2015.

Jia, X., Willard, J., Karpatne, A., Read, J. S., Zwart, J. A., Steinbach, M., and Kumar, V.: Physics-Guided Machine Learning for Scientific Discovery: An Application in Simulating Lake Temperature Profiles, ACMIMS Trans. Data Sci., 2, 1–26, https://doi.org/10.1145/3447814, 2021.

Jones, M. D. and Dee, S. G.: Global-scale proxy system modelling of oxygen isotopes in lacustrine carbonates: New insights from isotope-enabled-model proxy-data comparison, Quat. Sci. Rev., 202, 19–29, https://doi.org/10.1016/j.quascirev.2018.09.009, 2018.

https://doi.org/10.5194/egusphere-2026-2322
Preprint. Discussion started: 20 May 2026
© Author(s) 2026. CC BY 4.0 License.

Jones, M. D., Cuthbert, M. O., Leng, M. J., McGowan, S., Mariethoz, G., Arrowsmith, C., Sloane, H. J., Humphrey, K. K., and Cross, I.: Comparisons of observed and modelled lake δ18O variability, Quat. Sci. Rev., 131, 329–340, https://doi.org/10.1016/j.quascirev.2015.09.012, 2016.

Ladwig, R., Daw, A., Albright, E. A., Buelo, C., Karpatne, A., Meyer, M. F., Neog, A., Hanson, P. C., and Dugan, H. A.: Modular Compositional Learning Improves 1D Hydrodynamic Lake Model Performance by Merging Process-Based Modeling With Deep Learning, J. Adv. Model. Earth Syst., 16, e2023MS003953, https://doi.org/10.1029/2023MS003953, 2024.

Longo, W. M., Huang, Y., Russell, J. M., Morrill, C., Daniels, W. C., Giblin, A. E., and Crowther, J.: Insolation and greenhouse gases drove Holocene winter and spring warming in Arctic Alaska, Quat. Sci. Rev., 242, 106438, https://doi.org/10.1016/j.quascirev.2020.106438, 2020.

Mai, J.: Ten strategies towards successful calibration of environmental models, J. Hydrol., 620, 129414, https://doi.org/10.1016/j.jhydrol.2023.129414, 2023.

Marshall, C., Morrill, C., Dee, S., Jiang, Y., Kim, S., and Russell, J.: Proxy System Biases partially resolve long-standing paleoclimate data-model discrepancies in Tropical East Africa, Quat. Sci. Rev., 366, 109426, https://doi.org/10.1016/j.quascirev.2025.109426, 2025.

Martynov, A., Sushama, L., and Laprise, R.: Simulation of temperate freezing lakes by one-dimensional lake models: performance assessment for interactive coupling with regional climate models, 15, 2010.

Morrill, C., Small, E. E., and Sloan, L. C.: Modeling orbital forcing of lake level change: Lake Gosiute (Eocene), North America, Glob. Planet. Change, 29, 57–76, https://doi.org/10.1016/S0921-8181(00)00084-9, 2001.

Morrill, C., Meador, E., Livneh, B., Liefert, D. T., and Shuman, B. N.: Quantitative model-data comparison of mid-Holocene lake-level change in the central Rocky Mountains, Clim. Dyn., 53, 1077–1094, https://doi.org/10.1007/s00382-019-04633-3, 2019.

Mosquera, P. V., Batalla, M., Hampel, H., Vázquez, R. F., and Catalan, J.: Mixing regimes in tropical high-mountain Andean lakes, Limnol. Oceanogr., 70, 2872–2892, https://doi.org/10.1002/lno.70166, 2025.

New York State Department of Environmental Conservation Division of Water: Division of Water Monitoring Portal (Version 1.27.2025) [data set], https://experience.arcgis.com/experience/301748017d7d40649bc5082fc1c5365e/#data_s=id%3AdataSource_1-1949977d66f-layer-14%3A1791, last access: 12 April 2025.

NOAA/World Data Service for Paleoclimatology & Neotoma: National Centers for Environment Information Paleo Data Search [data set], https://www.ncei.noaa.gov/access/paleo-search/study/search.json?dataPublisher=NOAA%7CNeotoma&dataTypeId=13&headersOnly=true, last access: 30 September 2025.

https://doi.org/10.5194/egusphere-2026-2322
Preprint. Discussion started: 20 May 2026
© Author(s) 2026. CC BY 4.0 License.

NOAA National Centers of Environmental Information: Global Surface Summary of the Day - GSOD. 1.0 [data set], https://www.ncei.noaa.gov/access/search/data-search/global-summary-of-the-day?pageNum=1&pageSize=100&bbox=42.734,-79.935,41.871,-78.411, last access: 14 March 2026, 1999.

Parnell, A. C., Sweeney, J., Doan, T. K., Salter-Townshend, M., Allen, J. R. M., Huntley, B., and Haslett, J.: Bayesian Inference for Palaeoclimate with time Uncertainty and Stochastic Volatility, Journal of the Royal Statistical Society Series C: Applied Statistics, 64, 115–138, https://doi.org/10.1111/rssc.12065, 2015.

Parnell, A. C., Haslett, J., Sweeney, J., Doan, T. K., Allen, J. R. M., and Huntley, B.: Joint palaeoclimate reconstruction from pollen data via forward models and climate histories, Quaternary Science Reviews, 151, 111–126, https://doi.org/10.1016/j.quascirev.2016.09.007, 2016.

Perroud, M., Goyette, S., Martynov, A., Beniston, M., and Annevillec, O.: Simulation of multiannual thermal profiles in deep Lake Geneva: A comparison of one-dimensional lake models, Limnol. Oceanogr., 54, 1574–1594, https://doi.org/10.4319/lo.2009.54.5.1574, 2009.

Read, J. S., Jia, X., Willard, J., Appling, A. P., Zwart, J. A., Oliver, S. K., Karpatne, A., Hansen, G. J. A., Hanson, P. C., Watkins, W., Steinbach, M., and Kumar, V.: Process-Guided Deep Learning Predictions of Lake Water Temperature, Water Resour. Res., 55, 9173–9190, https://doi.org/10.1029/2019WR024922, 2019.

Sae-Lim, J. (Nadia), Konecky, B. L., Morrill, C., Michelutti, N., Grooms, C., and Smol, J. P.: Lake energy balance response to 21st century warming in the tropical high Andes, Glob. Planet. Change, 248, 104741, https://doi.org/10.1016/j.gloplacha.2025.104741, 2025.

Santos, E., Wagner-Riddle, C., Lee, X., Warland, J., Brown, S., Staebler, R., Bartlett, P., and Kim, K.: Use of the isotope flux ratio approach to investigate the C18 O16 O and13 CO2 exchange near the floor of a temperate deciduous forest, Biogeosciences, 9, 2385–2399, https://doi.org/10.5194/bg-9-2385-2012, 2012.

Steinman, B. A., Rosenmeier, M. F., Abbott, M. B., and Bain, D. J.: The isotopic and hydrologic response of small, closed-basin lakes to climate forcing from predictive models: Application to paleoclimate studies in the upper Columbia River basin, Limnol. Oceanogr., 55, 2231–2245, https://doi.org/10.4319/lo.2010.55.6.2231, 2010.

U.S. Geological Survey: National Water Information System data available on the World Wide Web (USGS Water Data for the Nation) [data set], https://dx.doi.org/10.5066/F7P55KJN, 2026.

Topness, R., Thomas, E., Fendrock, M., and Otiniano, G.: Lake proxy system model calibration framework (PRYSM v2.0) (v1.0.2), Zenodo [code], https://doi.org/10.5281/zenodo.20124941, 2026a.

Topness, R. and Thomas, E. K.: Physical and biogeochemical observations from Red Pond, New York, USA: 2021-2025, HydroShare [data set], http://www.hydroshare.org/resource/825c12377f0c4bad81af98b5947d87aa, 2026b.

Topness, R. and Thomas, E. K.: Physical and biogeochemical observations from Bear Lake, New York, USA: 2024-2026, HydroShare [data set], http://www.hydroshare.org/resource/672bb9941600460382dff2ca87319480, 2026c.

https://doi.org/10.5194/egusphere-2026-2322
Preprint. Discussion started: 20 May 2026
© Author(s) 2026. CC BY 4.0 License.

Topness, R., Thomas, E., Fendrock, M., and Otiniano, G.: Data and code for "Calibration guidelines and a runoff-isotope module for lake proxy system modeling (PRYSM v2.0)" (v1.0.0), Zenodo [data set], https://doi.org/10.5281/zenodo.19775686, 2026d.

Van Geldern, R. and Barth, J. A. C.: Optimization of instrument setup and post-run corrections for oxygen and hydrogen stable isotope measurements of water by isotope ratio infrared spectroscopy (IRIS), Limnol. Oceanogr. Methods, 10, 1024–1036, https://doi.org/10.4319/lom.2012.10.1024, 2012.

Virtanen, P., Gommers, R., Oliphant, T. E., Haberland, M., Reddy, T., Cournapeau, D., Burovski, E., Peterson, P., Weckesser, W., Bright, J., Van Der Walt, S. J., Brett, M., Wilson, J., Millman, K. J., Mayorov, N., Nelson, A. R. J., Jones, E., Kern, R., Larson, E., Carey, C. J., Polat, İ., Feng, Y., Moore, E. W., VanderPlas, J., Laxalde, D., Perktold, J., Cimrman, R., Henriksen, I., Quintero, E. A., Harris, C. R., Archibald, A. M., Ribeiro, A. H., Pedregosa, F., Van Mulbregt, P., SciPy 1.0 Contributors, Vijaykumar, A., Bardelli, A. P., Rothberg, A., Hilboll, A., Kloeckner, A., Scopatz, A., Lee, A., Rokem, A., Woods, C. N., Fulton, C., Masson, C., Häggström, C., Fitzgerald, C., Nicholson, D. A., Hagen, D. R., Pasechnik, D. V., Olivetti, E., Martin, E., Wieser, E., Silva, F., Lenders, F., Wilhelm, F., Young, G., Price, G. A., Ingold, G.-L., Allen, G. E., Lee, G. R., Audren, H., Probst, I., Dietrich, J. P., Silterra, J., Webber, J. T., Slavič, J., Nothman, J., Buchner, J., Kulick, J., Schönberger, J. L., De Miranda Cardoso, J. V., Reimer, J., Harrington, J., Rodríguez, J. L. C., Nunez-Iglesias, J., Kuczynski, J., Tritz, K., Thoma, M., Newville, M., Kümmerer, M., Bolingbroke, M., Tartre, M., Pak, M., Smith, N. J., Nowaczyk, N., Shebanov, N., Pavlyk, O., Brodtkorb, P. A., Lee, P., McGibbon, R. T., Feldbauer, R., Lewis, S., Tygier, S., Sievert, S., Vigna, S., Peterson, S., More, S., et al.: SciPy 1.0: fundamental algorithms for scientific computing in Python, Nat Methods, 17, 261–272, https://doi.org/10.1038/s41592-019-0686-2, 2020.

Wei, Z., Lee, X., Aemisegger, F., Benetti, M., Berkelhammer, M., Casado, M., Caylor, K., Christner, E., Dyroff, C., García, O., González, Y., Griffis, T., Kurita, N., Liang, J., Liang, M.-C., Lin, G., Noone, D., Gribanov, K., Munksgaard, N. C., Schneider, M., Ritter, F., Steen-Larsen, H. C., Vallet-Coulomb, C., Wen, X., Wright, J. S., Xiao, W., and Yoshimura, K.: A global database of water vapor isotopes measured with high temporal resolution infrared laser spectroscopy, Sci. Data, 6, 180302, https://doi.org/10.1038/sdata.2018.302, 2019.

Welker, J.M.: Isotopic (d18O) characteristics of weekly precipitation collected across the USA: An initial analysis with application to water source studies, Hydrological Processes, 14, 1449-1464, 2000.

Zhao, B., Castañeda, I. S., Bradley, R. S., Salacup, J. M., De Wet, G. A., Daniels, W. C., and Schneider, T.: Development of an in situ branched GDGT calibration in Lake 578, southern Greenland, Org. Geochem., 152, 104168, https://doi.org/10.1016/j.orggeochem.2020.104168, 2021.